Publication Year	2019
Acceptance in OA@INAF	2021-03-15T12:18:45Z
Title	Occurrence of F region echoes for the polar cap SuperDARN radars
Authors	Koustov, Alexander V.; Ullrich, Sydney; Ponomarenko, Pavlo V.; Nishitani, Nozomu; MARCUCCI, Maria Federica; et al.
DOI	10.1186/s40623-019-1092-9
Handle	http://hdl.handle.net/20.500.12386/30699
Journal	EARTH, PLANETS AND SPACE
Number	71

Earth, Planets and Space

FRONTIER LETTER

Open Access

Occurrence of F region echoes for the polar cap SuperDARN radars

Alexander V. Koustov[1*], Sydney Ullrich[1], Pavlo V. Ponomarenko[1], Nozomu Nishitani[2], Federica M. Marcucci[3] and William A. Bristow[4]

Abstract

Observations by six Super Dual Auroral Radar Network (SuperDARN) polar cap radars, three in the northern hemisphere and three in the southern hemispheres, are considered to assess F region echo occurrence rates over solar, season, and day cycles and to establish relationship between the echo occurrence rate and the background electron density and plasma flow velocity magnitude. The echo occurrence rate is shown to increase toward the solar cycle maximum, more distinctly on the nightside, consistent with a general trend of the background electron density. Over the last 5 years, the echo occurrence rates decline at a rate of 5–10% per year. The pattern of seasonal and diurnal variations in echo occurrence is found to be consistent with previous SuperDARN publications. Minor dips in echo occurrence rate are observed in winter solstices, and these are related to an overall decrease in the electron density. In most of the time sectors, the echo occurrence rate increases with the electron density but only up to a certain threshold value after which the dependence saturates. The level of the saturation depends on season, local time, and average plasma flow velocity magnitude. For the summer daytime observations, the echo occurrence rate correlates with variations of both electron density and plasma flow velocity magnitude.

Keywords: Polar cap radars, Echo occurrence rate, F region electron density, $\mathbf{E} \times \mathbf{B}$ plasma flow magnitude

Introduction

Super Dual Auroral Radar Network (SuperDARN) high-frequency (HF) radars are widely used for studying plasma flow patterns in the Earth's ionosphere (e.g., Chisham et al. 2007; Nishitani et al. 2019). The radars send pulses into the ionosphere, obliquely with respect to the Earth's surface, and receive echoes from various ionospheric heights after radio waves are backscattered by plasma irregularities in the decameter range. Of special interest are ionospheric echoes from the F region because the Doppler velocity of these echoes is the line-of-sight (LOS) component of the $\mathbf{E} \times \mathbf{B}$ plasma flow (e.g., Gillies et al. 2018; Drayton et al. 2005). Since decameter F region plasma irregularities are strongly stretched along the Earth's magnetic field lines (e.g., Tsunoda 1988), the backscatter is only efficient if HF radio waves propagate almost perpendicular to them. This "orthogonality" condition is achievable at HF owing to strong radio wave refraction in the ionosphere. The amount of refractive radio wave bending depends on the electron density distribution in the ionosphere, both horizontally and vertically (e.g., Villain et al. 1984). Having sufficiently high electron density in the ionospheric F region is one of the crucial conditions for the echo detection with the SuperDARN radars (e.g., Koustov et al. 2014, 2018).

To detect ionospheric echoes in SuperDARN observations, in addition to satisfying the orthogonality condition, irregularities must be present. It is generally accepted that F region decameter irregularities are generated through various plasma instabilities. The gradient drift (GD) plasma instability is the most likely mechanism at high latitudes (e.g., Fejer and Kelley 1980; Tsunoda 1988; Gondarenko and Guzdar 2006). The GD instability at the F region heights occurs when there is a plasma density gradient in the direction of the $\mathbf{E} \times \mathbf{B}$ plasma drift. A stronger electric field and sharper density gradient are preferable for the instability excitation;

*Correspondence: sasha.koustov@usask.ca
[1] Department of Physics and Engineering Physics, University of Saskatchewan, Saskatoon, SK, Canada
Full list of author information is available at the end of the article

Springer Open

© The Author(s) 2019. This article is distributed under the terms of the Creative Commons Attribution 4.0 International License (http://creativecommons.org/licenses/by/4.0/), which permits unrestricted use, distribution, and reproduction in any medium, provided you give appropriate credit to the original author(s) and the source, provide a link to the Creative Commons license, and indicate if changes were made.

under these conditions, the chances for the detection of ionospheric echoes in SuperDARN observations are expected to increase.

Past studies have shown that the SuperDARN F region echo occurrence rates vary significantly from one radar to another, and they depend on the time of a day, season, and phase of the solar cycle (e.g., Ruohoniemi and Greenwald 1997; Milan et al. 1997; Danskin et al. 2002; Koustov et al. 2004; Prikryl et al. 2010; Bristow et al. 2011; Ghezelbash et al. 2014a, b; Lamarche and Makarevich 2015). The reasons for these variations are not well understood, but knowledge of them is important for operation of HF communication, remote sensing, and surveillance systems.

A number of SuperDARN studies focused on the role of two factors affecting occurrence of F region echoes, enhanced electron density, and electric field (Milan et al. 1997, 1999; Danskin et al. 2002; Ghezelbash et al. 2014b; Koustov et al. 2014, 2018; Lamarche and Makarevich 2015). It was confirmed that the electron density is indeed a crucial factor for echo detection while, unexpectedly, the strength of the electric field seems to be less important (Ghezelbash et al. 2014b; Koustov et al. 2014). One weakness of the previous work in this direction is the limited data set of joint observations by SuperDARN and supplemental instruments measuring ionospheric plasma parameters.

One approach to improving our knowledge on the reasons for occurrence of F region SuperDARN echoes is assessing general trends in echo occurrence rate and comparing those with variations of ionospheric parameters that are expected to control the onset of echoes (Koustov et al. 2004; Kane et al. 2012; Ghezelbash et al. 2014b; Lamarche and Makarevich 2015). Recent studies by Ghezelbash et al. (2014b) and Lamarche and Makarevich (2015) focused on investigation of such trends for the polar cap SuperDARN radars in the Northern (NH) and Southern (SH) hemispheres, respectively. The polar cap radars are of particular importance because over the last decade of relatively low solar activity they have been a major data source for construction of global-scale convection maps. Importantly, more than 10 years of data are available in the NH and more than 5 years in the SH, allowing an investigation of the solar cycle effect. Some limited information on occurrence of SuperDARN echoes in the polar cap has been also given by Ponomarenko et al. (2010), Prikryl et al. (2010), Bristow et al. (2011) and Koustov et al. (2014).

This study expands the work by Ghezelbash et al. (2014b) and Lamarche and Makarevich (2015) with two goals: (1) comparative statistics of the F region echo occurrence rates for the polar cap SuperDARN radars in both hemispheres and (2) more detailed investigation of how the echo occurrence rate is controlled by electron density and electric field variations at these latitudes.

Previous studies of HF echo occurrence versus electron density/electric field in the ionosphere

Generally, the power of coherent HF echoes is proportional to the average electron density in the scattering volume, intensity of ionospheric irregularities, the aspect angle attenuation factor, and some other factors, for example, the azimuthal angle of radar observations (Uspensky et al. 1994). Having a stronger return signal provides better chances for echo detection. The electron density influences echo detection in two ways: directly, as the echo amplitude is proportional to the electron density (Uspensky et al. 1994) and indirectly, through control of the aspect angle of radio waves reaching the scattering volume.

A number of SuperDARN studies acknowledge that the electron density affects the echo occurrence rate because it controls the amount of ionospheric refraction and defines whether the orthogonality condition is met (e.g., Milan et al. 1997; Danskin et al. 2002; Nishitani et al. 2019). It is important to realize that with the electron density increase the echo power from a specific range starts to saturate because the amount of refraction exceeds what is needed to achieve the orthogonality in the central part of the scattering layer, so that the echoes can only be received from limited portions at the bottom or top of the layer (e.g., Uspensky et al. 1994; Koustov et al. 2018). A decrease in the span of accessible heights might decrease the echo detection rate because the ionospheric irregularities might exist only in a limited range of heights.

In line with the expected effects of the electron density, Koustov et al. (2014, 2018) showed that with the electron density increase, the SuperDARN echo occurrence rate increases but starting from a certain threshold value, the rate saturates. The threshold electron density was shown to depend on the radar frequency and the time of day. In these publications, no attempt has been made to separate the electron density effect from the concurrent changes of the electric field magnitude that might affect the echo detection rate as well.

The electric field magnitude can affect the echo occurrence by changing the intensity of ionospheric decameter irregularities. This effect is well known for a case of E region irregularities driven by the GD instability (e.g., Fejer and Kelley 1980; Schlegel 1996). To what extent this effect works for a case of F region SuperDARN echoes is not known. Danskin et al. (2002) showed no significant effect for the auroral zone SuperDARN Hankasalmi radar. Koustov et al. (2014) also showed that with the

electric field increase, the echo occurrence rate for the Rankin Inlet (RKN) polar cap radar does not increase significantly. On the other hand, Fukumoto et al. (2000) showed that the power of SuperDARN echoes increases with the LOS velocity (which is a component of the $\mathbf{E} \times \mathbf{B}$ plasma drift) and thus, the dependence upon the electric field is expected. Ghezelbash et al. (2014b) showed good correlation in diurnal variations of the echo occurrence rate and electric field for summer observations with the RKN radar.

Observations: radar field of views and approach to occurrence computation

This study involves observations with six SuperDARN polar cap radars, Inuvik (INV), Rankin Inlet (RKN) and Clyde River (CLY) in the NH and Dome C East (DCE), McMurdo (MCM), and South Pole Station (SPS) in the SH. Figure 1a, b shows the fields of view (FoVs) of these radars in the NH and SH, respectively, starting from 500 km (ending at 2000 km for the SH radars). Within each field of view, the colored boxes show specific beams and gates from which data will be discussed. Table 1 lists these beams and gates. The coloring scheme for the radars adopted in Fig. 1a, b will be consistently used in the following diagrams, whenever data for a specific radar are considered.

In Fig. 1a for the NH radars, the beams selected have a common area at geographic latitudes and longitudes around 72°N and 100°W, respectively. The area of overlap is quite extensive. A smaller "common" region for the radars would correspond to INV beam 15, CLY beam 5, and RKN beam 2, all at about the same range gates ~24. Ghezelbash et al. (2014b) discussed echo occurrence rates for this limited region for observations in 2013. In line with more general objectives of the present study, this study considers data in more extended regions for all three radars. However, one advantage of observations in the smaller common area, that will be used in this study, is a possibility to estimate the $\mathbf{E} \times \mathbf{B}$ vector by merging data from three independent directions with the standard merge technique that does not employ any modeling, contrary to the traditional Ruohoniemi and Baker (1998) approach. We note that for the beams selected, the RKN radar LOS is close to the magnetic meridians while the CLY and INV radars' LOS are closer to the magnetic parallels.

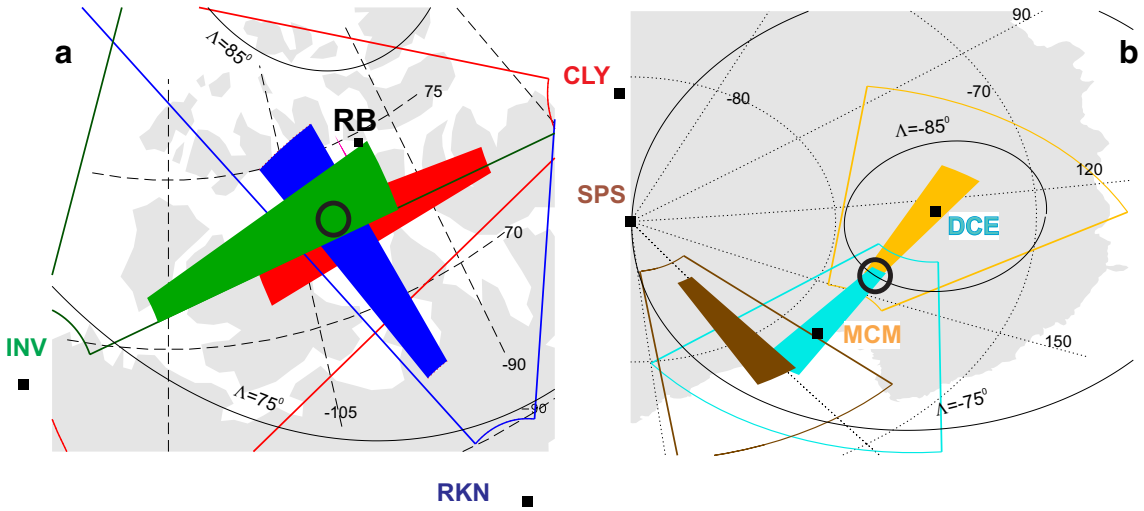

Fig. 1 Fields of view (FoVs) of the polar cap SuperDARN radars in the **a** Northern and **b** Southern hemispheres selected for the analysis. Specific beams (see Table 1) and gates (10–30) are shown by the colored boxes. The coloring is as follows: green—Inuvik (INV), blue—Rankin Inlet (RKN), red—Clyde River (CLY), brown—South Pole (SPS), light blue—Dome-C East (DCE), and orange—McMurdo (MCM). The solid gray lines are contours of constant magnetic latitude of 75° and 85°. The circle in **a** is the approximate location of a region where the plasma flow velocity magnitude was estimated while in **b** is simply an area of radar observations overlap

Table 1 Radar beams and gates of various SuperDARN radars selected for the analysis

	INV	RKN	CLY	DCE	MCM	SPS
Beams	13–15	1–3	4–6	10–12	6–8	3–5
Gates	10–30	10–30	10–30	10–30	10–30	15–30

In the SH, Fig. 1b, the DCE and MCM radars also have a "common" area for the beams selected at near range gates ~10 (black circle). The range gates 10–30 were selected for the analysis of these radars. This is to match the range coverage of the NH radars and, on the other hand, to cover all typical ranges of the echoes (for echo band determination, see next section). The overlap area in the SH is then at the near edge of the selected echo detection zones. The SPS radar monitors echoes in a somewhat different region from those of the DCE and MCM radars. In addition, its beams are oriented roughly along the magnetic parallels while the DCE and MCM beams are aligned roughly with the meridians, similarly to the RKN radar in the NH.

In the analysis below, while computing the echo occurrence rate, we use the local solar time assigned roughly to the middle of the echo detection zone. This implies some uncertainty for the azimuthally looking radars such as INV, CLY, and SPS, but for relatively small span of range gates considered, the uncertainty is not very large.

The echo occurrence rate was computed as a ratio of the number of registered echoes in selected beams and gates to the total number of possible echo detections in the same gates over the same period. 15-min averaging intervals were considered, and the ratios were presented in percent (the ratio of one is equivalent to 100%).

Figure 2 presents a contour plot for the echo occurrence rate on a "range gate-local time (LT)" plane for range gates 0–50 of the INV radar. Data for February 2014 were considered. According to Fig. 2, the echo occurrence rate is enhanced in a band that extends from roughly gate 10 to gate 30. The band is not uniform. It is observed at closer range gates in the afternoon (15–18 LT) and at farther range gates between 20 and 30 in the midnight and morning sectors (22–08 LT). These changes of the range of the observed echoes are caused by regular diurnal variations in the F region electron density. They are consistent with what has been reported for the MCM radar by Lamarche and Makarevich (2015). The maximum occurrence rates are close to 60% between 15 and 05 LT with generally smaller values outside this interval, i.e., during midnight and morning hours, with a significant drop between 05 and 08 LT corresponding to the local dawn. In this study, we consider a relatively wide band of radar ranges so that the latitudinal variations of the band location are smoothed out. We comment that limited echo occurrence rate enhancement can be seen in Fig. 2 at small range gates of ~0–10 between 09 and 11 LT. These are very likely E region echoes; they are of no interest in this study.

Plots similar to Fig. 2 have been produced for all months and all radars under investigation. We found that the bands of enhanced echo occurrence rate correspond to range gates 10–30, similarly to Fig. 2, consistently. Some plots showed limited in time and minor spatial departures, both to closer and farther ranges, but these were limited occasions. One exception is the SPS radar, for which the nighttime observations show persistent occurrence of echoes at near range gates corresponding to detection of E region echoes, as described by Makarevich et al. (2015) and Forsythe and Makarevich (2017). These echo bands often extend to large range gates (~20), and it is difficult to determine the location of the gates with pure E and pure F region echo detection. For the SPS radar, we selected the band of range gates as 15–30.

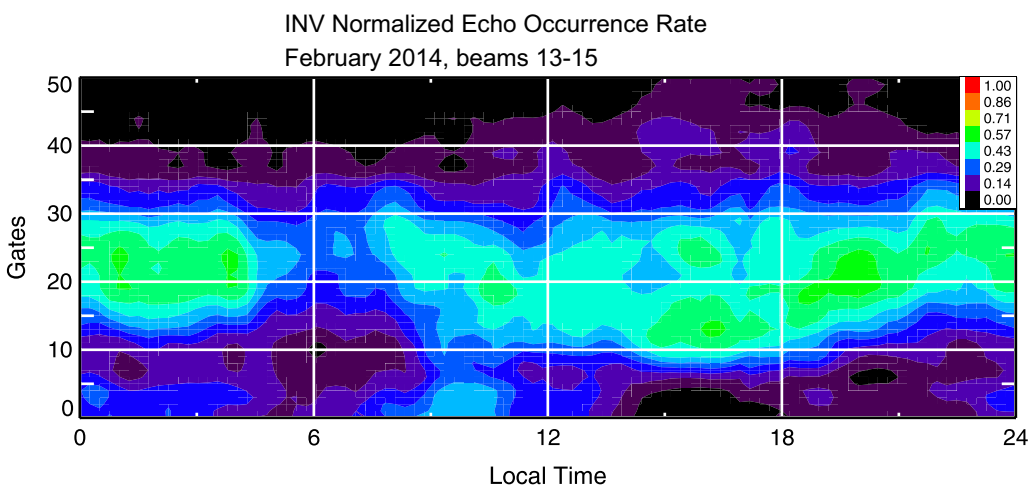

Fig. 2 A contour plot of the echo occurrence rate versus local time for the Inuvik radar in beams 13–15 and gates 0–50. Solar local time was counted for the radar location, LT = UT − 7. Data at all radar operating frequencies were considered

Typical pattern of echo occurrence on a month-local time plane

To assess the echo occurrence rates for each radar quantitatively, we consider data in specific range gates (as described above) and compute echo occurrence rate in these range gates for each 15-min interval of a day. Obtained data are then smoothed over a day, month, or season by applying a sliding boxcar filter of appropriate length. For example, to make a judgement on the seasonal variations, we apply a filter of a 60-day length.

Echo occurrence rates averaged over monthly periods are shown in Fig. 3a, b on a "season (month) − local time" plane for the INV (northern hemisphere) and DCE (southern hemisphere) radars, respectively. Observations include 5 consecutive years (2013–2017) of data. We note that the white box in Fig. 3b for the DCE observations in 2017 indicates an extended period with no suitable data. The radar was operating at this time but used very high frequency of >14 MHz. The respective echo occurrence rates are very low compared to observations at "traditional" SuperDARN frequencies of 10–12 MHz, and for this reason, these "non-standard" observations are not considered here.

One obvious conclusion from the plots of Fig. 3a, b is that the occurrence rates are larger on the dayside as compared to the nightside. Second, there is a general decrease in echo occurrence toward 2017, which is the year of the lowest solar activity in solar cycle 24. Third, one can recognize that the occurrence rates are enhanced during winter near-noon and afternoon hours. Also, the INV data show some occurrence enhancements at near-noon summer hours. Such enhancements are not seen in the DCE data.

One interesting and important feature of the data in Fig. 3a, b is a tendency for higher echo occurrence rate during later LT hours in the dusk sector and earlier LT hours in the dawn sector as the season progresses from winter to equinoxes. At the equinoxes, the occurrence maxima are achieved near midnight. As the season progresses from summer to winter, the occurrence rate maxima are achieved at earlier local time in the dusk sector and later local time in the dawn sector so that the overall regions of enhanced occurrence in Fig. 3a, b look like a diamond with corners at winter-noon and equinox-midnight hours. Prikryl et al. (2010), Kane et al. (2012) and Ghezelbash et al. (2014a) described similar patterns for the auroral zone SuperDARN radars. An important feature of the data in Fig. 3a, b is that, consistent with Ghezelbash et al. (2014a), the regions with enhanced echo occurrence follow the changes in the location of the solar terminator with the solar zenith angles around 90°, shown by white lines.

Plots similar to Fig. 3a, b have been produced for all 6 polar cap radars for all years of their operation. On a season-LT plane, the polar cap SuperDARN radars show about the same patterns of echo occurrence as the auroral zone SuperDARN radars.

Although the season-LT plots contain all the information on the long- and short-term variations in the echo occurrence rate, we focus below on some salient features by considering appropriate line plots.

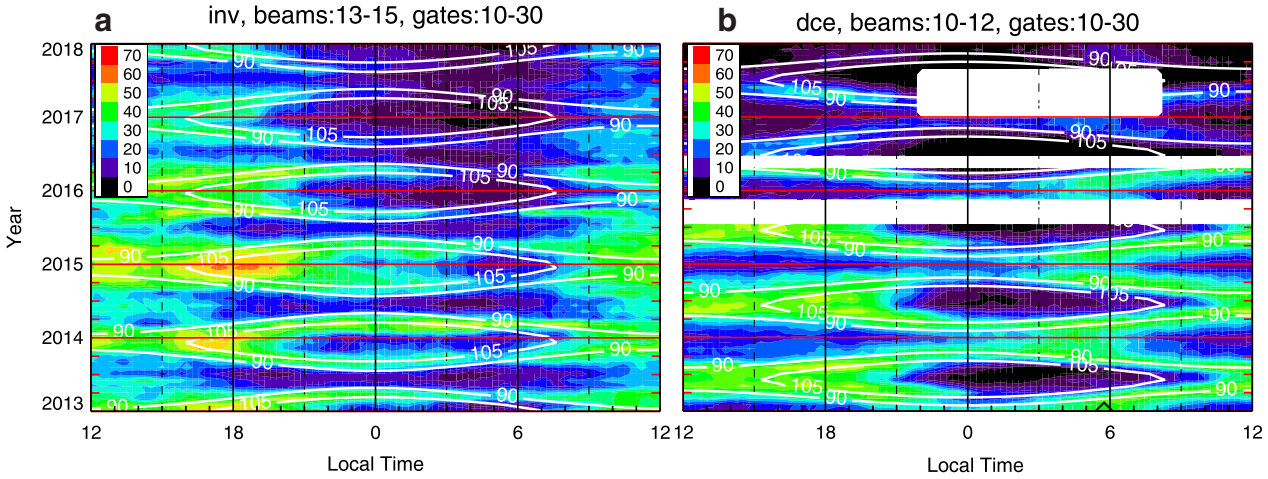

Fig. 3 A contour plot of the echo occurrence rate versus the solar local time for **a** Inuvik (INV), LT = UT − 7 and **b** Dome-C East (DCE), LT = UT + 10, SuperDARN radar observations in 2013–2017. Data at all radar operating frequencies were considered. The echo detection zones are depicted in Fig. 1a, b. Solid white lines are contours of the local solar zenith angles of 90° and 105°

Solar cycle trend in echo occurrence rates

To illustrate the long-term trends in echo occurrence rate, we consider more extended observations in the NH, between 2008 and 2018, Fig. 4. We focus in our presentation on the afternoon data collected between 12 and 18 local time although data in other time sectors have been investigated as well. This period was chosen because it has the highest echo detection rate and the largest set of electron density data.

In Fig. 4, we first present data on the solar activity level as characterized by the solar radio emission flux at 10.7 cm, Fig. 4a. In Fig. 4a, the raw daily data taken from the National Geophysical Data Center website (http://www.ngdc.noaa.gov/) are shown by gray-greenish line.

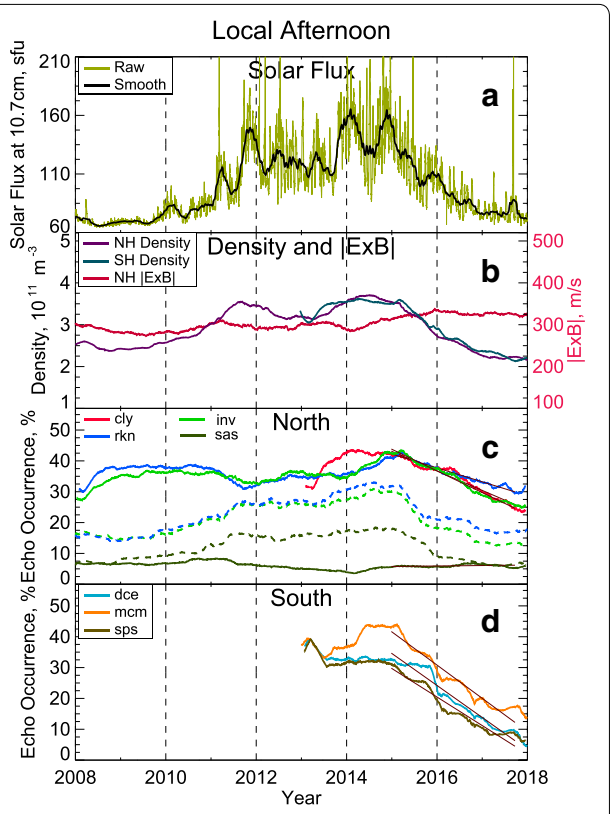

Fig. 4 Data on the polar cap SuperDARN echo occurrence and Sun's activity between January 2008 and December 2017. **a** The solar 10.7-cm radio flux. **b** The electron density at the F layer peak in the NH and SH and the $\mathbf{E} \times \mathbf{B}$ flow magnitude in the area of radar observations in the NH, both parameters inferred from SuperDARN measurements. **c** Solid lines are radar echo occurrence rates in percent (daily afternoon values, 15 ± 3 h of local time) smoothed by applying a running 1-year boxcar filter for the NH polar cap radars at CLY, RKN, and INV. The decline in the echo occurrence rate in 2014–2017 is assessed by the linear fit lines and their slopes are reported in Table 2. Dashed lines show the occurrence rate for the INV and CLY radars in the midnight sector (0 ± 3 h). **d** The same as **c** but for the DCE, MCM, and SPS radars in the southern hemisphere

To smooth high variability of the daily values, we applied a boxcar filter of 60-day length, see black line. Clearly, the period under consideration starts with reduced solar activity that is followed by a steep rise between 2011 and 2012. This is the expected time for the solar cycle 24 maximum based on the fact that solar cycle 23 peaked in 2001. The January 2012 peak was not strong, and the activity started subsiding afterward. However, two additional and stronger peaks in the solar activity occurred around January 2014 and January 2015. Subsequently, the solar activity has been declining.

Figure 4b shows the afternoon ($15 \text{ LT} \pm 3$ h) sector electron density at the F region maximum, purple curve, as inferred from the RKN radar elevation angle measurements in the area of RKN, INV, and CLY radar echo detection using the technique by Ponomarenko et al. (2011). These data will be discussed later. We note that the electron density correlates with the solar activity changes, with an obvious overall increase during the years of increased solar activity, 2012–2015. Figure 4b also shows the afternoon electron density at the F region maximum in the SH (dark blue-green line), inferred from the DCE radar observations by the same technique. Here, the data are only available for the period of 2013–2017. This curve is close to that of the NH electron density curve.

Figure 4b also shows the afternoon $\mathbf{E} \times \mathbf{B}$ plasma flow magnitudes (crimson line) inferred by merging LOS velocity data from the NH radars. The velocity magnitude does not change significantly, staying between 250 and 300 m/s. One would generally expect that the polar cap flows are faster during the years of high solar activity because of stronger solar wind drivers of the flow during these periods. The velocity magnitude in Fig. 4b has a very subtle local enhancement in 2012 but it then dropped by about 10% in 2014, the year of the strongest F10.7 cm flux. The reason for the rise is not clear. We note that although SuperDARN data do show the flow velocity increase in response to the solar wind driver intensification (e.g., Koustov et al. 2015), the effect is not very strong. Moreover, once the SuperDARN data are averaged without consideration of the Interplanetary Magnetic Field (IMF) conditions, the enhancement is very weak (Koustov et al. 2013). It is a very likely that the velocity decrease in 2014 is the result of stronger flow variability during this period and averaging of the velocity data over various IMF conditions.

Figure 4c shows the echo occurrence rate for the polar cap radars in the NH. The RKN and INV data cover the entire period under consideration while the CLY data are only available for the period of 2013–2017 corresponding roughly to the solar cycle 24 maximum and its declining phase. The local afternoon echo occurrence rates for

RKN and INV, shown by the solid lines, are relatively steady at a level of ~ 35% from 2008 to 2015; there is a very slight increase estimated as ~ 0.7% per year. After 2015, these radars, as well as the CLY radar, show very clear decrease. The rates of this decrease are very close to each other; they are on the order of 5% per year. We quantified the rate of the decline by making a linear fit to the occurrence curves between January 2015 and December 2017 for four local time sectors. The slopes of the linear fit are given in Table 2 in percent per year.

While investigating the data, we discovered that the echo occurrence rate increases toward the solar cycle maximum are strongest for the nighttime. The dashed lines in Fig. 4c represent the echo occurrence rates for the INV and RKN radars at nighttime (0 LT ± 3 h). These data show much steeper increase of the echo occurrence rate toward the solar maximum, on the order of 2.5% per year, while the rate of the decline afterward is somewhat less than to that on the dayside.

Figure 4c also shows the afternoon (solid dark green line) and nighttime (dashed dark green line) echo occurrence rates for the auroral zone Saskatoon (SAS) SuperDARN radar, between 2008 and 2018. We considered the SAS radar beams 2–3 and range gates 10–30. These data are presented to compare the solar cycle effects in the auroral zone and in the polar cap. Consistent with Ghezelbash et al. (2014a), no significant variation in the echo occurrence rate is seen for the afternoon echoes with the typical rates at a level of 5–7%. A minor decline is seen in echo occurrence rates for the years near the solar cycle maximum consistent with Ghezelbash et al. (2014a), their Fig. 4b, who considered SAS data for the previous solar cycle. The nighttime SAS rates are larger, roughly by a factor of 2, and the trends are obvious with a clear increase toward the solar cycle maximum and a decline afterward. The slopes of the trends are close to those for the nighttime observations in the polar cap. One can conclude that the echo occurrence rates for the SuperDARN radars in the polar cap and the auroral zone show comparable solar cycle trends for the nighttime while the effects are slightly stronger in the polar cap in the afternoon.

Figure 4d shows the afternoon (15 LT ± 3 h) echo occurrence rates for the polar cap radars in the SH. Here, the data are only available for the period of 2013–2017. Consistent with observations in the NH, the echo occurrence rates show a very clear decrease. The rates of this decrease are very close to each other and are somewhat faster than those in the NH. We also quantified the rate of the decline by making a linear fit to the curves between January 2015 and December 2017. The slopes of the linear fit are given in Table 2 in percent per year.

One general conclusion from Table 2, based on the bottom line representing the average values over a day, is that the rates of the decline are very comparable and stay in between 4% and 9% per year depending on the radar. The strongest decline is for the DCE and MCM radars located and monitoring the ionosphere at the largest geographic latitudes. In terms of time of day, there is no clear time sector that shows strongest decline, although the SH radars experience a faster decline on the dayside.

Data presented in Fig. 3a, b indicate that the seasonal and diurnal changes are inter-related, and separation of these variations is difficult. Nevertheless, we proceed below by applying averaging over respective time domains to reveal the tendencies.

Seasonal variations

To assess the seasonal effects, we computed average echo occurrence rates over a 6-h period from 12 LT to 18 LT and plotted these values for the period of 2013–2017 when data for both hemispheres were available, Fig. 5. Again, the afternoon period was chosen because it has the highest echo detection rate and the largest set of electron density data. We note that echo occurrence rates averaged over 24 h periods show variations similar to those shown in Fig. 5.

Table 2 Linear fit line slopes of the echo occurrence decline in 2015–2017 (Fig. 4c, d) for various time* sectors and radars. The time sectors were selected according to the local solar time ± 3 h**

	Echo occurrence decrease slope in % per year (bands)						
	CLY	RKN	INV	DCE	MCM	SPS	AVG
Night (0 ± 3) LT	− 8.19	− 5.30	− 6.16	− 6.69	− 5.59	− 4.76	− 6.11
Dawn (9 ± 3) LT	− 5.91	− 2.52	− 5.17	− 8.16	− 5.86	− 6.04	− 5.61
Day (12 ± 3) LT	− 5.65	− 5.55	− 7.50	− 10.32	− 10.39	− 6.58	− 7.67
Dusk (18 ± 3) LT	− 7.63	− 5.13	− 5.53	− 9.85	− 11.16	− 8.11	− 7.90
Afternoon (15 ± 3) LT	− 6.3	− 4.5	− 7.0	− 10.4	− 10.8	− 9.2	− 8.03
Average (0 ± 24) LT	− 6.84	− 4.63	− 6.09	− 8.75	− 8.25	− 6.37	− 6.82

The bottom and the right lines show the average value of the slopes

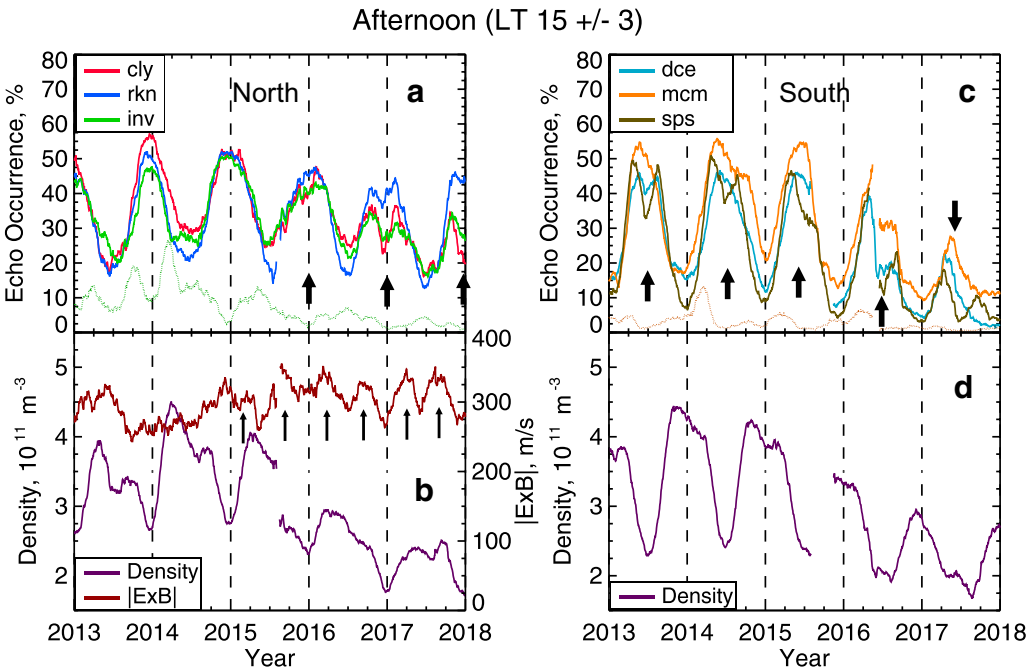

Fig. 5 Line plots of the echo occurrence rate averaged between 12 and 18 LT (smoothed by applying a running 60-day boxcar filter) versus time of the year for **a** the northern hemisphere INV, CLY, and RKN radars and **c** the southern hemisphere MCM, SPS, and CLY radars. Dashed lines in **a** and **c** are the ground scatter occurrence rate for the INV and MCM radars, respectively. **b** and **d** are the average F region peak electron density between 12 and 18 LT (smoothed by applying a running 60-day boxcar filter), purple line, and the $\mathbf{E} \times \mathbf{B}$ magnitude (smoothed by applying a running 60-day boxcar filter, gray line in **b** only), both versus time of the year. Arrows in **a** and **c** point at local, minor echo occurrence minima in winter. Arrows in **b** indicate time equinoctial $\mathbf{E} \times \mathbf{B}$ plasma flow magnitude enhancements for some years of observations

Figure 5a shows the afternoon echo occurrence rates for the INV, RKN, and CLY radars in the NH while Fig. 5b shows the afternoon echo occurrence rates for the MCM, SPS, and DCE radars in the SH for 2013–2017. The NH radars show, more or less consistently, overall winter maxima. There is a tendency for these winter enhancements to be more extended (in terms of time) toward the end of the period under consideration so that the bell-shaped curves are "narrower" in 2014. This feature will be discussed later. The winter overall enhancements are centered on winter solstices but the actual maxima are slightly shifted toward the equinoctial time for winters of 2016 (only for CLY), 2017, and 2018. A possible reason for this effect will be discussed later. The SH radars show similar tendencies with the occurrence rate maxima being somewhat away from the winter solstices. This is most clear for the SPS radar. The occurrence rate "dips" in winter are marked in Fig. 5 by arrows. The winter-solstice occurrence rates are still higher than those in summer.

The bottom plots in Fig. 5b, d show the average F region peak electron density as inferred from RKN measurements in the NH (Fig. 5b) and DCE measurements in the SH (Fig. 5d). For the NH data in Fig. 5a, the $\mathbf{E} \times \mathbf{B}$ magnitudes are also given.

The density curves in Fig. 5b, d show clear minima in winter. The seasons for the electron density maxima are not so well defined. In the NH, the maxima are clearly at the equinoxes in 2013–2015. In 2016 and 2017, the equinoctial maxima are less obvious, especially in 2016 with the fall maximum being completely missed. The SH data have some indications of the equinoctial maxima in 2013–2016 but single summer maxima are seen in 2017 and 2018.

Comparing the echo occurrence data of Fig. 5a, c and respective electron density data of Fig. 5b, d, one can conclude that, roughly to speak, there is an anti-correlation of the two parameters. This conclusion is in contrast with the results reported in the previous section where the solar cycle variations between the two parameters were found to be in phase. Reasons for this difference will be discussed later.

Diurnal variations

To assess diurnal variations of echo occurrence, Fig. 6 plots echo occurrence rates as a function of local time for the NH and SH polar cap radars and four separate

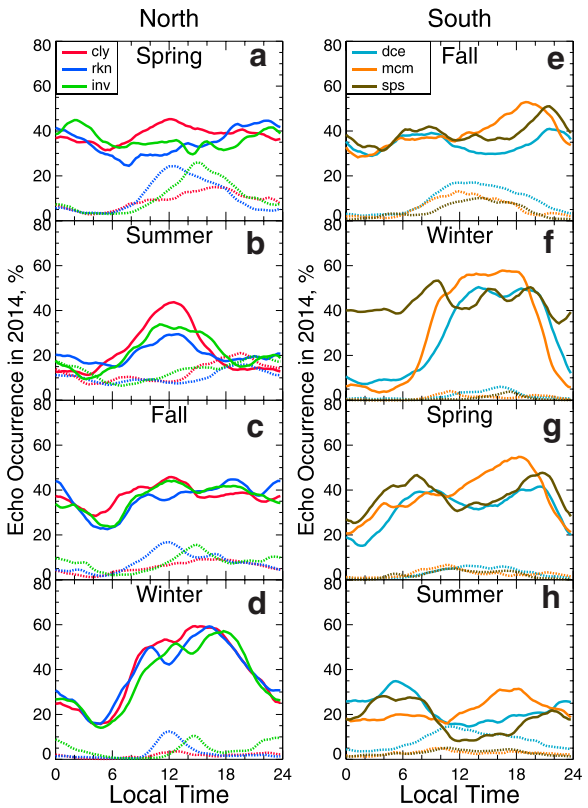

Fig. 6 Line plots of the echo occurrence rate in percent (median values over 15-min intervals in 2014 smoothed by applying a running 1-h boxcar filter) versus time of a day for each season in the Northern (NH, left panels) and Southern (SH, right panels) hemispheres. The right and left panels are data over the same periods, e.g., panel **a** for the spring in the NH covers the same period as panel **b** for the fall in the SH

seasons in 2014 (as a representative year of data). The plots are organized in such a way that data for one season (and three radars) in one hemisphere are matched with data for the "opposite" season (and three radars) in the other hemisphere so that, horizontally, the plots correspond to the same time period of observations.

In Fig. 6, individual radars in the NH (first column) show similar trends; the red, blue, and green curves are very close to each other. In the SH, consistency between the radars is less evident. The DCE radar has mostly smaller echo occurrence rate than the MCM radar as the orange curves (for MCM) in Fig. 6e–h are typically above the light blue lines (for DCE). This is expected because the DCE radar waves need much more refraction to achieve the orthogonality condition as the magnetic field lines are inclined away from the radar (contrary to the incline toward to all other polar cap radars). Figure 6f shows that while daytime—dusk echo occurrence rates are at comparable levels of ~30–40% and drop down dramatically in the other time sectors for the DCE and MCM radars, the SPS radar shows lower occurrence rates during daytime and significantly higher rates during nighttime. This discrepancy requires additional investigation. We believe that the nighttime echoes are often coming from the E region. In absence of elevation angle measurements, we cannot confirm this hypothesis.

Data of Fig. 6 indicate that diurnal variation in echo occurrence is less pronounced near the equinoxes where the rates are smoothly varying at a level of 30–40%. Rates for spring are slightly higher during afternoon and dusk, in both hemispheres. In the NH, there is a decrease in occurrence at dawn, which is not seen in the SH data.

Summer trends in the NH and SH data are quite different. In the NH, near noon enhancements are seen (Fig. 6b) while, in the SH, the MCM occurrence is maximized at dusk and the DCE occurrence is maximized at dawn. These MCM and DCE maxima correspond to either of the radars being located on the nightside with central beams looking toward dayside. The SPS radar has both dawn and dusk maxima. These maxima correspond to SPS observations along the average plasma flow.

The data in winter are consistent between the hemispheres, with the exception of the SPS data that might be affected by the E region scatter (as explained above). In winter, the echo occurrence rate increases during prenoon hours and stays at same level until dusk. Nighttime occurrence rates are significantly reduced, and the effect is stronger in the SH where complete darkness stays for a longer time than in the NH.

Trends in echo occurrence rate as a function of electron density and E × B magnitude

For the NH observations considered in this study, information on the electron density and $\mathbf{E}\times\mathbf{B}$ plasma flow velocity is available, allowing us to assess how these factors might influence the occurrence rate. In this assessment, cumulatively for the entire data set, the data were split according to four seasons (spring, summer, fall, winter) and four time sectors (dawn, noon, dusk, midnight). The seasons were defined as periods covering observations during ± 45 days from the day of a solstice or an equinox. The time sectors were defined as ± 3 h from the center of a local time sector (e.g., 12 ± 3 LT for the noon/daytime sector).

To get estimates of the $\mathbf{E}\times\mathbf{B}$ plasma flow magnitude (in the text to follow, we will refer to this quantity as the $\mathbf{E}\times\mathbf{B}$ magnitude) in the ionosphere, we considered those 15-min intervals for which the velocity measurements from at least one pair, CLY–RKN or INV–RKN, were available. For these intervals, the median LOS velocity was determined for each radar. The velocity data in beams and gates corresponding to the "common

point" (black circle in Fig. 1a) were considered. Then, the merged velocity vectors for each radar pair were produced assuming that the measured radar velocity is the cosine component of a full $\mathbf{E} \times \mathbf{B}$ vector (Greenwald et al. 1995). When merged velocity vectors were available for both radar pairs, the average value was considered. For some of the intervals, information on the electron density at the F region maximum was available from RKN elevation angle measurements (as described by Ponomarenko et al. 2011).

Figure 7a–d plots the echo occurrence rate for the CLY and INV radars versus the electron density for the noon time sector in each season. Data in common area of three radar observations (gates 22–23 for CLY and gates 24–25 for INV) were considered. The curves were obtained by considering a boxcar filter with a length of 0.8×10^{11} m^{-3} applied to a scatter plot of the echo occurrence versus electron density. In each panel of Fig. 7a–d, individual curves correspond to 3 bins of the $\mathbf{E} \times \mathbf{B}$ magnitude: 50–250 m/s, 250–400 m/s, and > 400 m/s.

In Fig. 7a–d, the curves in every individual panel show very similar trends. Importantly, the curves show higher occurrence rates at larger $\mathbf{E} \times \mathbf{B}$ magnitudes signifying that this factor affects the echo detection rate and "response" to the electron density. Another interesting feature in these plots is that the shape of the curves changes with season. In summer (Fig. 7b), the overall occurrence rate increase with the density is obvious until density values above $\sim 4 \times 10^{11}$ m^{-3} where signatures of a saturation in the dependence are evident. In fall and spring (Fig. 7a, c), the increasing part is steeper, and the saturation is achieved at much smaller electron density of $\sim 3 \times 10^{11}$ m^{-3}. For winter (Fig. 7d), the increasing part of the curves is short so that the occurrence rate stays at about the same level for electron densities above $(2 - 2.5) \times 10^{11}$ m^{-3}. There is also a tendency for

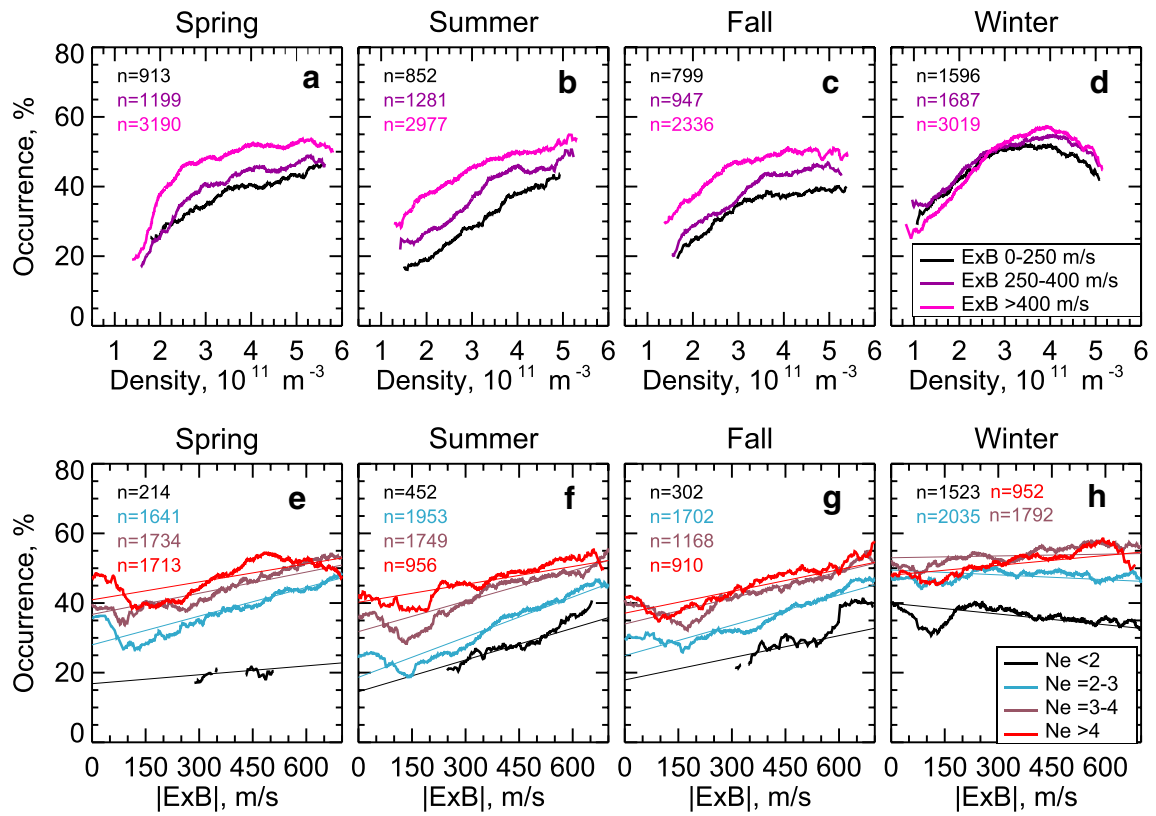

Fig. 7 **a**–**d** Smoothed average values of the echo occurrence rate for the Clyde River (CLY) and Inuvik (INV) radars as a function of the F region peak electron density (inferred from concurrent and co-located Rankin Inlet (RKN) elevation angle measurements). All noon sector data collected in 2013–2017 were considered. Individual curves in each panel correspond to three bins of the $\mathbf{E} \times \mathbf{B}$ plasma flow magnitude of 50–250 m/s, 250–400 m/s, and > 400 m/s. Also presented in each panel is the total number of 15-min intervals available to build each curve. **e**–**h** Smoothed average values of the echo occurrence rate for the CLY and INV radars versus the $\mathbf{E} \times \mathbf{B}$ plasma flow magnitude. Individual curves in each panel correspond to four bins of the F region peak electron density of $< 2 \times 10^{11}$ m^{-3}, $(2 - 3) \times 10^{11}$ m^{-3}, $(3 - 4) \times 10^{11}$ m^{-3}, and $> 4 \times 10^{11}$ m^{-3}. The linear fit lines are shown for each set of points

the echo occurrence rate to decrease at large electron density values of $> 4 \times 10^{11}\,\mathrm{m}^{-3}$. The negative slope of the dependence at largest electron densities is actually more common than Fig. 7 might suggest. It is typical for other time sectors in equinoxes and especially in winter. Summer data show weaker dependence for dusk and no dependence for dawn and midnight. The negative slope of the echo occurrence rate versus the electron density is an interesting effect. Its understanding requires more data analysis beyond the targets of the present study. One possibility is a systematic shift of the optimal echo detection zone to shorter ranges, away from rather limited area where the echo occurrence rates were computed. In winter, this effect might be enhanced by generally low background electron density, outside polar cap patches. Another possibility is that an increase in occurrence of ground scatter is blocking chances to detect ionospheric echoes.

An important conclusion from this analysis is that the strongest response of echo occurrence rate to an increase of the electron density takes place at near noon in summer. This conclusion is consistent with the analysis by Ghezelbash et al. (2014b) who reported a strong correlation of electron density and RKN echo occurrence rates for near-noon summer observations.

Figure 7e–h plots the echo occurrence rate versus the $\mathbf{E} \times \mathbf{B}$ magnitude for the CLY and INV radars for all seasons and near-noon hours. The curves were obtained by considering a boxcar filter with the length of 100 m/s applied to scatter plots of echo occurrence versus $\mathbf{E} \times \mathbf{B}$ magnitude. In each panel of Fig. 7e–h, individual curves correspond to four bins (if available) of the F region peak electron density of $< 2 \times 10^{11}\,\mathrm{m}^{-3}$, $(2\text{–}3)\times 10^{11}\mathrm{m}^{-3}$, $(3\text{–}4)\times 10^{11}\mathrm{m}^{-3}$ and $> 4 \times 10^{11}\,\mathrm{m}^{-3}$. The curves in Fig. 7e–g show a similar trend of larger overall echo occurrence rates for larger electron densities, as expected, signifying that the electron density is an important factor affecting the echo occurrence rate. Since the trends are almost linear, we computed a linear fit line to each curve. Parameters of the fit line for these plots are presented in Table 3. The slopes of the linear fit vary; stronger slopes are seen for intermediate bins of the electron density. Data of Fig. 7e–g indicate that the "response" of the echo occurrence rate to the $\mathbf{E} \times \mathbf{B}$ magnitude increase is stronger in summer and at larger densities. Analysis of similar plots for other time sectors showed that the slopes are smaller there with almost no occurrence rate increase in the dawn and night sectors.

A general conclusion from the above analysis is that there are differences between winter and summer observations at noon and dusk. In summer, the echo occurrence rate responds to both the electron density and electric field increase while in winter it responds only to the electron density increase and the dependence saturates at fairly low densities.

Table 3 Slopes in %/(km/s) and intercepts in % of a linear fit to scatter plots of echo occurrence rate versus E × B magnitude for near noon observations

Density bin	Spring slope/ intercept	Summer slope/ intercept	Fall slope/ intercept	Winter slope/ intercept
$N_e < 2 \times 10^{11}\mathrm{m}^{-3}$	8.7/16	30.6/14	21.3/17	−10.3/39
$2 \le N_e < 3 \times 10^{11}\mathrm{m}^{-3}$	27.5/27	38.4/18	29.0/24	−4.6/49
$3 \le N_e < 4 \times 10^{11}\mathrm{m}^{-3}$	20.3/36	29.2/31	24.9/33	1.7/53
$N_e > 4 \times 10^{11}\mathrm{m}^{-3}$	17.2/40	17.2/40	20.8/37	9.5/48

Discussion

The data presented in this study show a complicated pattern of long- and short-term variations of the SuperDARN HF echo occurrence in the polar cap. The patterns are largely consistent with previous studies where limited data sets were considered (Prikryl et al. 2010; Ghezelbash et al. 2014b; Koustov et al. 2014; Lamarche and Makarevich 2015).

Now we discuss the extent to which the reported long- and short-term variations in echo occurrence are controlled by the electron density and $\mathbf{E} \times \mathbf{B}$ plasma flow magnitude changes.

Solar cycle trends

The data presented in Fig. 4 demonstrate that the occurrence rate of the SuperDARN F region polar cap echoes varies throughout the solar cycle with overall enhancement during high solar activity, similar to what was reported for the auroral zone SuperDARN radars by Ruohoniemi and Greenwald (1997), Kane et al. (2012) and Ghezelbash et al. (2014a). Although not discussed, the data by Ghezelbash et al. (2014a) show faster echo occurrence rate decrease on the declining phase of the solar cycle 23 as compared to that on the developing phase. For the polar cap radars at RKN and INV, the slope of the occurrence rate increase is estimated as ~ 2% per year for nighttime conditions (the strongest effect, Fig. 4c) and the slope of the decrease is ~ 5–10% per year, as reported in Table 2. Over the same period, the echo occurrence rate increase and decline for the auroral zone Saskatoon (SAS) radar (computed for the central beams 2–3 and range gates 10–30) at nighttime (strongest effect as well) are ~ 1% and ~ 4% per year, respectively. Thus, the solar cycle effect is comparable for the SuperDARN radars in the polar cap and auroral zone with slightly stronger effect in the polar cap.

In terms of the factors determining the echo occurrence rates for SuperDARN, Greenwald (2013) was probably the first author who explicitly stated that long-term changes in the number of SuperDARN echoes are due to variations of the ionospheric electron density affecting the amount of possible refraction experienced by HF radio waves. The data presented in Fig. 4 are consistent with this hypothesis. The $\mathbf{E} \times \mathbf{B}$ magnitude data of Fig. 4b also show that, on average, this parameter does not increase toward the solar cycle maximum, and thus, it cannot be the major factor responsible for the solar cycle variation in the polar cap echo occurrence.

According to Table 2, the echo occurrence decay (in recent years) is faster in the SH. This can be related to a stronger decline in the F region electron densities at higher geographic (and geomagnetic latitudes) where the SH polar cap radars monitor echoes. For testing this suggestion, the smoothed density curve for the SH daytime condition (estimated from DCE elevation data by applying the method by Ponomarenko et al. (2011)) indicates that the SH densities were close to those in the NH. We hypothesize that perhaps the electron density threshold for the SH echo detection is more stringent. For example, the DCE radar requires more refraction to reach the orthogonality condition. This larger threshold might be also the reason for faster occurrence rate decline in the SH.

Seasonal variations

This study showed strong seasonal effects in the occurrence rate of polar cap SuperDARN echoes, consistent with previous reports for other SuperDARN radars (Ruohoniemi and Greenwald 1997; Koustov et al. 2004; Kane et al. 2012; Ghezelbash et al. 2014a, b; Lamarche and Makarevich, 2015). The major identified feature is the preferential echo occurrence in winter as compared to summer such that the seasonal changes in the electron density and echo occurrence rate are in antiphase. This implies that electron density cannot be responsible for seasonal variations in echo occurrence. Interestingly, the NH electron density shows maxima away from the winter solstices, closer to equinoctial time (Fig. 5b). The echo occurrence does not show matched equinoctial maxima. This feature can be explained by the fact that the densities in the equinoxes are often at or above the saturation threshold (Fig. 7).

Figure 5 shows minor differences in the shape of winter curves at the beginning and at the end of the interval considered for the NH radars with single maxima centered on winter solstices in 2013–2016 but with minor local minima in winter solstices in 2017–2018 so that here the echo occurrence maxima are shifted toward equinoxes. One possible explanation of this "splitting" of the maxima and formation of echo occurrence winter dips toward the end of the period considered is the overall decline of the electron density. Data on the electron density in Fig. 5b support this explanation. Indeed, the "splitting" begins once the electron density becomes close to 2×10^{11} m^{-3}, a typical threshold value for SuperDARN echo detection (Koustov et al. 2014; 2018). The SH hemisphere data, notably the SPS data, show the winter dips in echo occurrence quite often. This is consistent with the expected smaller winter densities in the SH hemisphere where radar observations were performed at larger geographic latitudes.

Since the echo occurrence rate depends on the $\mathbf{E} \times \mathbf{B}$ magnitude in the ionosphere, at least for the daytime (Fig. 7), one can think that this factor can affect the seasonal variation. Data presented in Fig. 7b do not support this hypothesis as the $\mathbf{E} \times \mathbf{B}$ magnitude shows local minor enhancements for some equinoctial time (see arrows). These local enhancements are not strong and, unsurprisingly, no matched enhancements in echo occurrence are seen, with the exception of observations in 2017.

The data presented in Fig. 5 indicate much smaller echo occurrence rates in summer. This cannot be related to variations of the F region electron density and electric field, as seen in Fig. 5. Traditionally, this feature is explained by the effect of the solar radiation smoothing out the electron density gradients and prohibiting the development of the GD instability (Ruohoniemi and Greenwald 1997; Lamarche and Makarevich 2015). There is no doubt that the effect is present. We think, however, that the summer decrease in echo occurrence rate is also enhanced by the frequent occurrence of sporadic E layers (MacDougall et al. 2000) blocking echo detection with HF radio waves or damping the F region irregularity growth (Milan et al. 1999). Another potential effect is the occurrence of strong ground scatter echoes which prevents the identification of ionospheric echoes. To illustrate the importance of this factor, we show the occurrence rate for ground scatter, for the INV radar in the NH, and for the MCM radar in the SH by dotted lines in Fig. 5a, c. The rates are smaller, especially in the SH, but their enhancements correlate with the periods of lowest occurrence rate for ionospheric echoes, see for example, the NH data for 2014–2016. Another interesting feature in the ground scatter data of Fig. 5a is spikes in echo occurrence at equinoxes in 2013 and 2014. We think that frequent presence of ground scatter during these periods resulted in more "narrow" bell-shaped curves for CLY and INV in 2013 and 2014 as compared to other years when no such spikes were observed (2015–2017).

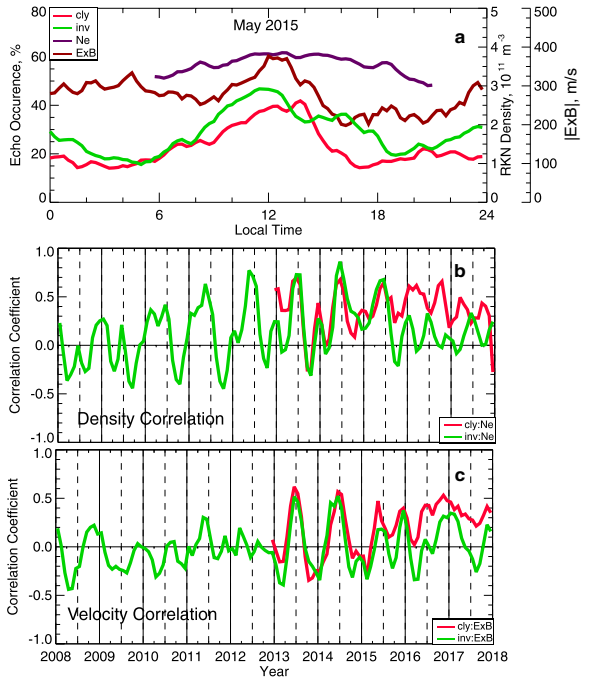

Fig. 8 **a** Line plots of the echo occurrence rate in percent (15-min values averaged over the entire month) versus time of a day in May 2015 for the Inuvik (INV) and CLY radars and the electron density at the F region peak as inferred from Rankin Inlet (RKN) elevation angle data (purple line) and the $\mathbf{E} \times \mathbf{B}$ plasma flow magnitude (black line) in the area of joint RKN–INV–CLY observations. Nighttime RKN data on the electron density are not considered. **b** Correlation coefficients between diurnal variations of the INV and CLY echo occurrence rate and the electron density at the F region peak. **c** Correlation coefficients between diurnal variations of the INV and CLY echo occurrence rate and the $\mathbf{E} \times \mathbf{B}$ magnitude

Diurnal trends

Diurnal variations of the polar cap echo occurrence rate reported in this study are generally consistent with previous publications (e.g., Ghezelbash et al. 2014b; Lamarche and Makarevich 2015). Ghezelbash et al. (2014b) associated them with diurnal variations of the electron density. Our Fig. 6 shows strong near noon and dusk enhancements of echo occurrence in the NH for all seasons (as well as for winter in the SH). During these periods, the electron density is largest for the NH (e.g., Themens et al. 2017). To further investigate this correlation, we compare the monthly averaged diurnal trends for the electron density and echo occurrence rate in Fig. 8.

Figure 8a explains the approach to the comparison. Here, the INV and CLY echo occurrence rate and the electron density inferred from RKN measurements are shown as a function of local time for May 2015. We note that no reliable nighttime electron density data are available. While considering the RKN data on the electron density, we discovered that RKN-based electron densities are often well above the statistically average values known, for example, from ionosonde measurements at Resolute Bay (e.g., Themens et al. 2017). This happens because the elevation angles are small at low electron densities and the deterministic component of the phase signal being mixed with the strong random noise sometimes assumes negative values. In this case, the signal phase is flipped by 2π by the standard SuperDARN software. This automatically translates to unrealistically large electron density values through the procedure by Ponomarenko et al. (2011). To avoid any confusion, these data were simply not considered.

The echo occurrence rate and electron density diurnal trends are assessed by computing the correlation coefficient between the curves R_{Ne}. It is ~0.8 for the INV radar in this specific month. Figure 8a also shows the curve for the $\mathbf{E} \times \mathbf{B}$ magnitude. The correlation coefficient in diurnal trends of the echo occurrence rate and the $\mathbf{E} \times \mathbf{B}$ magnitude $R_{E \times B}$ is not as good, only ~0.3, for the INV radar.

Similar correlation analysis was performed for every month of joint RKN, INV, and CLY observations in 2008–2017. Figure 8b, c presents correlation coefficients R_{Ne} and $R_{E \times B}$, respectively. Clearly, they vary significantly, from positive values of ~0.8, implying good correlation, to negative values implying no correlation or even anti-correlation. The correlation coefficients R_{Ne} are positive in most summers (denoted by vertical dashed lines). Some excursions to positive values are seen for winters, but the numeric values are rather low. The correlation coefficients $R_{E \times B}$ are seldom positive. Some degree of correlation can be seen for summers, but the values are low, below 0.4, with the exception of the 2013–2014 data.

In summer, the density-occurrence positive correlation is highly expected, based on the data of Fig. 7b. This was the case (Fig. 8b). In winter, the correlation coefficients were smaller than in summer. This is also expected as the response of echo occurrence rate to electron density increase saturates at low electron densities (Fig. 7d). Our data thus show weaker correlation of echo occurrence rate and electron density than that reported by Ghezelbash et al. (2014b) for the RKN radar observations over Resolute Bay. We believe that this can be for two reasons. First, in this study the INV and CLY data were collected at ranges of optimal echo detection so that the deficiency in the density is less critical as compared to the RKN observations near the far edge of the echo detection zone studied by Ghezelbash et al. (2014b). Second, the nighttime data have been excluded from the comparison in the present study, and thus typically positive correlations during transitions from darkness to daylight and from daylight to darkness have been excluded.

The above correlation analysis confirms the important role of the electron density in shaping the diurnal

variation of the polar cap radar echo occurrence. An interesting fact further strengthening this conclusion is that the correlation coefficients R_{Ne} in Fig. 8b attain larger values (envelope of upper values in Fig. 8b) during the years of high solar activity with generally higher electron densities.

Positive correlation of the $\mathbf{E} \times \mathbf{B}$ magnitude and echo occurrence rate in Fig. 8c indicates that this factor can be important during some periods, for example, in 2013–2015. Ghezelbash et al. (2014b) reported that the effect is strong in summer. Our data of Fig. 8c do have some years with good correlation in summer, but there is no significant correlation for many other years.

In the considerations above, we discussed seasonal and diurnal variations separately. However, the data of Fig. 3 and similar plots in Kane et al. (2012), Ghezelbash et al. (2014a) and Lamarche and Makarevich (2015) indicate that the dependencies are interrelated and probably need to be considered simultaneously.

Ghezelbash et al. (2014a) suggested that the diamond-like pattern of enhanced echo occurrence on a "month-MLT" plane (similar to our Fig. 3) is consistent with the onset of a "gray ionosphere" with strong spatial non-uniformity of the electron density distribution at times close to sunset or sunrise. For these periods, the ionosphere provides favorable conditions for HF radio wave propagation and decameter irregularity production. This notion has been articulated by Ghezelbash et al. (2014a, b) by showing that the line of ~90° solar zenith angle nearly coincides with the month-MLT trends in the enhancement of echo occurrence. The solar-zenith angle lines presented in Fig. 3a, b demonstrate the same features. We note that for the SPS radar, seasonal transition from a complete darkness to a complete sunlight and back happens over relatively short period, and consistent with this, the pattern of enhanced echo occurrence on a month-LT plane (not presented in this paper) has only weak signatures of a "diamond" structure.

An alternative explanation of the diamond-like patterns is a combination of the seasonal variations in the electron density and solar irradiation, as strongly argued by Lamarche and Makarevich (2015). One challenging point in this scenario is the lack of correlation (zero or negative correlation coefficients) between the electron density and echo occurrence rate diurnal trends in equinoxes for many years of observations, Fig. 8. This is consistent with the report by Ghezelbash et al. (2014b) for the RKN radar observations over Resolute Bay. In equinoxes, the electron density is high enough for echo detection all day (perhaps, slightly decreased at nighttime). Since densities are generally high (and the saturation state on the occurrence–density curve is achieved), other factors, such as terminator-related electron density inhomogeneity and $\mathbf{E} \times \mathbf{B}$ magnitude, affect the echo occurrence rate. It is our opinion that both scenarios, presence of the solar terminator and seasonal variations of the electron density and solar illumination, are very likely at play.

Our observations in the SH revealed one interesting feature that is difficult to explain. It has been mentioned that the SH polar cap radars do not show summer noon echo occurrence enhancements, contrary to the NH radars. One possible explanation of the effect is the onset of ground scatter blocking ionospheric echo detection. Figure 6 contains information on the ground scatter occurrence for every radar, dotted lines of respective color. One can notice that ground scatter can cause effective "decrease" in ionospheric echo detection in the SH but not in the NH where no near-noon enhancement of ground scatter is seen. However, combined ionospheric plus ground scatter curve (can be done by eye examination) would not show strong near-noon maxima for all SH radars. One of the hypotheses is that perhaps the irregularity production is not effective in the SH owing to stronger smoothing effect of the solar radiation for observations at much higher geographic latitudes with longer solar illumination time.

Summary and conclusions

1. In this study, we investigated, for the first time, solar cycle trends in the F region echo occurrence rate for the polar cap SuperDARN radars by considering 10 years of observations in the northern hemisphere (for 3 radars) and 5 years of observations in the southern hemisphere (for 3 radars). The rates are shown to increase toward the solar cycle 24 maximum and decline afterward. The effect is (1) stronger at nighttime and (2) is comparable (slightly stronger) to that observed by the Saskatoon radar selected to represent SuperDARN observations in the auroral zone. For the declining phase of the solar cycle 24, the polar cap radars in both hemispheres show a decrease in the echo occurrence rate by 5–10% per year with a somewhat faster decline in the southern hemisphere. The long-term trends in the overall echo occurrence rate and the F region electron density are similar. No correlation was found with long-term changes of the $\mathbf{E} \times \mathbf{B}$ flow magnitude. The observations support the notion that electron density is the major factor influencing overall SuperDARN echo occurrence rates in the polar cap.
2. Seasonal variations of the echo occurrence rate were investigated on a longer data set than previous studies and by considering concurrent observations in both hemispheres. It was confirmed that the echo

occurrence rates are highest in winter and equinoxes and persistently smallest in summer of respective hemispheres. For the first time, minor differences in the seasonal trends in the hemispheres were identified. While the NH data show mostly a symmetric bell-shaped distribution with the maximum centered at winter solstices, the SH data show asymmetric curves often with minor local dips at winter solstices so that local seasonal maxima are shifted toward the equinoctial time. The overall decrease in occurrence of the polar cap SuperDARN echoes in summer is related to the solar radiation effects of increasing the D region HF radio wave absorption, and deterioration in production of F region decameter irregularities. Another reason is more frequent occurrence of sporadic E layers blocking F region echo detection. The echo occurrence minor dips at winter solstices are related to significant decrease of the F region electron density, especially at nighttime.

3. Diurnal variations of the echo occurrence rate were investigated on a longer data set and by considering observations in both hemispheres. It was confirmed that the pattern of polar cap-enhanced echo occurrence rate on a season-LT plane is similar to that of the auroral zone radars. It is of a diamond shape with enhanced rates at noon in winter and at midnight in equinoxes. The pattern can be explained by a combination of several factors including diurnal and seasonal variations on F region electron density and electric field and seasonal changes of solar irradiation of the polar cap ionosphere. Another factor is the presence of the solar terminator-related gray ionosphere within the radar observational area.
4. We identified minor differences in the shape of the diurnal variations of echo occurrence in the hemispheres. These are as follows: (1) The SH data show dawn–dusk enhancements in all seasons except of winter while these are not recognizable in the NH data. (2) The NH data show near-noon enhancement in summer while the maxima are shifted toward dawn and dusk sectors for the SH data so that at noon there is rather a minor decrease in echo occurrence. The NH echo occurrence enhancement correlates well with increased electron density and, to a lesser extent, with enhancement of the plasma flow velocity magnitude.
5. Response of the polar cap F region echo occurrence rate to an increase in the F region peak electron density (in both hemispheres) and $\mathbf{E}\times\mathbf{B}$ plasma flow magnitude (in the NH) were investigated by considering a significantly larger data set of the electron density and $\mathbf{E}\times\mathbf{B}$ flow. The database was created by involving the elevation angle measurements by the RKN (NH) and DCE (SH) radars and crossed-beam velocity measurements by the RKN, INV, and CLY radars (NH). The dataset allowed us, for the first time, to investigate the occurrence rate response for various seasons and times of the day while the data are binned according to the electron density and $\mathbf{E}\times\mathbf{B}$ flow magnitude. No nighttime observations were considered since the elevation angle measurements are sometimes compromised with the currently implemented technique of the electron density estimates. We confirmed that the polar cap echo occurrence rate response to the ionospheric electron density increase is highly nonlinear with a saturation effect at large densities. The winter, equinox, and summer threshold values are approximately $\sim 2\times10^{11}\,\mathrm{m}^{-3}$, $\sim 3\times10^{11}\,\mathrm{m}^{-3}$, and $\sim 4\times10^{11}\,\mathrm{m}^{-3}$, respectively, for the NH polar cap radars, consistent with previous SuperDARN studies where F peak electron densities were available in spatially limited ionospheric regions. A new peculiar feature noticed is a decreasing trend of echo occurrence rate at largest observable electron densities. It was shown, for the first time, that for daytime and dusk observations (1) the saturation level of echo occurrence is larger for stronger $\mathbf{E}\times\mathbf{B}$ magnitudes and (2) the increasing part of the dependence is much steeper in winter and equinoxes. The latter finding is consistent with the reported correlation in diurnal variations of echo occurrence rate and electron density.

Abbreviations

CLY: Clyde River; DCE: Dome C East; FoV: field of view; GD: gradient drift; HF: high frequency; INV: Inuvik; LOS: line-of-sight; LT: local time; MCM: McMurdo; MLT: magnetic local time in hours; NH: northern hemisphere; RKN: Rankin Inlet; SAS: Saskatoon; SH: southern hemisphere; SPS: South Pole Station; SuperDARN: Super Dual Auroral Radar Network.

Acknowledgements

Continuous funding of the SuperDARN radars by National Scientific Agencies of Australia, Canada, China, France, Italy, Japan, Norway, South Africa, United Kingdom, and the United States of America is appreciated. The current research would be impossible without ongoing support from the Canadian Foundation for Innovation, Canadian Space Agency's Geospace Observatory (GO Canada) continuation initiative to the U of Saskatchewan radar group and NSERC Discovery grant to AVK. AVK acknowledges funding from the Institute for Space-Earth Environmental Research (ISEE), Nagoya University while he visited the Nagoya University and worked on the paper. For this study, essential are contributions from the Dome C East, McMurdo and South Pole radars. The Dome C East radar was installed in the framework of a French-Italian collaboration and is operated by the Institute for Space Astrophysics and Planetology-Instituto di Astrofisica e Planetologia Spaziali of the Istituto Nazionale di Astrofisica (INAF-IAPS) with the support of Italian National Research Council (CNR) and National Program for Antarctic Research (PNRA).

Authors' contributions
AVK drafted the manuscript. SU performed extensive analysis of the data provided by PVP (electron density measurements), MFM (DCE raw radar data), and WAB (MCM and SPS raw radar data). NN contributed to the radar data analysis. All authors read and approved the final manuscript.

Funding
A.V.K. was supported by NSERC Discovery (Canada) grant (RGPIN 03741-2016) and International Joint Research Program of the Institute for Space-Earth Environmental Research, Nagoya University, S.U. was funded by NSERC CREATE (Canada) program (RS346079), P.V.P. was funded by NSERC Discovery (Canada) Grant (RGPIN 1774-2002), N.N. was supported by JSPS KAKENHI (Japan) Grants 16H06286 and 18KK0099, F.M.M. was funded by the PNRA (Italy) Grant 14_00085, W.A.B. was funded by NSF, Directorate of Geosciences (USA) Grants 1443504 and 1341902.

Availability of data and materials
SuperDARN data can be obtained from https://superdarn.ca.

Ethics approval and consent to participate
Not applicable.

Competing interests
The authors declare that they have no competing interests.

Author details
[1] Department of Physics and Engineering Physics, University of Saskatchewan, Saskatoon, SK, Canada. [2] Institute for Space-Earth Environmental Research, Nagoya University, Nagoya, Aichi, Japan. [3] Institute for Space Astrophysics and Planetology, Rome, Italy. [4] University of Alaska Fairbanks, Fairbanks, AK, USA.

Received: 4 April 2019 Accepted: 16 October 2019
Published online: 28 October 2019

References

Bristow WA, Spaleta J, Parris RT (2011) First observations of ionospheric irregularities and flows over the south geomagnetic pole from the Super Dual Auroral Radar Network (SuperDARN) HF radar at McMurdo Station, Antarctica. J Geophys Res Space Phys 116:A12325. https://doi.org/10.1029/2011JA016834

Chisham G, Lester M, Milan SE, Freeman MP, Bristow WA, Grocott A, McWilliams KA, Ruohoniemi MJ, Yeoman TK, Dyson PL, Greenwald RA, Kikuchi T, Pinnock M, Rash JPS, Sato N, Sofko GJ, Villain J-P, Walker ADM (2007) A decade of the Super Dual Auroral Radar Network (SuperDARN): Scientific achievements, new techniques and future directions. Surv Geophys 28:33–109. https://doi.org/10.1007/s10712-007-9017-8

Danskin DW, Koustov AV, Ogawa T, Nishitani N, Nozawa S, Milan SE, Lester M, Andre D (2002) On the factors controlling the occurrence of F-region coherent echoes. Ann Geophys 20:1399–1413. https://doi.org/10.5194/angeo-20-1385-2002

Drayton RA, Koustov AV, Hairston MR, Villain J-P (2005) Comparison of DMSP cross-track ion-drifts and SuperDARN line-of-sight velocities. Ann Geophys 23:2479–2486. https://doi.org/10.5194/angeo-23-2479-2005

Fejer BG, Kelley MC (1980) Ionospheric irregularities. Rev Geophys 18:401–454. https://doi.org/10.1029/RG018i002p00401

Forsythe VV, Makarevich RA (2017) Global view of the E region irregularity and convection velocities in the high-latitude southern hemisphere. J Geophys Res Space Phys 122:2467–2483. https://doi.org/10.1002/2016JA023711

Fukumoto M, Nishitani N, Ogawa T, Sato N, Yamagishi H, Yukimatu AS (2000) Statistical study of Doppler velocity and echo power around 75° magnetic latitude using data obtained with the Syowa East HF radar in 1977. Adv Polar Upper Atmos Res 14:93–102

Ghezelbash M, Fiori RAD, Koustov AV (2014a) Variations in the occurrence of SuperDARN F region echoes. Ann Geophys 32:147–156. https://doi.org/10.5194/angeo-32-147-2014

Ghezelbash M, Koustov AV, Themens DR, Jayachandran PT (2014b) Seasonal and diurnal variations of PolarDARN F region echo occurrence in the polar cap and their causes. J Geophys Res Space Phys 119:10426–10439. https://doi.org/10.1002/2014JA020726

Gillies RG, Perry GW, Koustov AV, Varney RH, Reimer AS, Spanswick E, St-Maurice J-P, Donovan E (2018) Large-scale comparison of polar cap ionospheric velocities measured by RISR-C, RISR-N, and SuperDARN. Radio Sci. https://doi.org/10.1029/2017RS006435

Gondarenko NA, Guzdar PN (2006) Nonlinear three-dimensional simulations of mesoscale structuring by multiple drives in high-latitude plasma patches. J Geophys Res Space Phys 111:A08302. https://doi.org/10.1029/2006JA011701

Greenwald RA (2013) Refraction and SuperDARN. Paper presented at 2013 Annual SuperDARN workshop, 26–31 May 2013, Moose Jaw, Saskatchewan, Canada, 34

Greenwald RA, Baker KB, Dudeney JR, Pinnock M, Jones TB, Thomas EC, Villain J-P, Cerisier J-C, Senior C, Hanuise C, Hunsuker RD, Sofko G, Koehler J, Nielsen E, Pellinen R, Walker ADM, Sato N, Yamagishi H (1995) DARN/SUPERDARN: a global view of the dynamics of high-latitude convection. Space Sci Rev 71:761–796. https://doi.org/10.1007/BF00751350

Kane TA, Makarevich RA, Devlin JC (2012) HF radar observations of ionospheric backscatter during geomagnetically quiet periods. Ann Geophys 30:221–233. https://doi.org/10.5194/angeo-30-221-2012

Koustov AV, Sofko GJ, André D, Danskin DW, Benkevitch LV (2004) Seasonal variation of HF radar F region echo occurrence in the midnight sector. J Geophys Res Space Phys 109:A06305. https://doi.org/10.1029/2003JA010337

Koustov AV, Fiori RAD, Aboolizadeh, Z (2013) Averaged plasma flows in the polar cap inferred from SuperDARN data. Paper presented at SuperDARN-2013 workshop, 26–1 May 2013, Moose Jaw, Saskatchewan, Canada

Koustov AV, Ponomarenko PV, Ghezelbash M, Themens DR, Jayachandran PT (2014) Electron density and electric field over Resolute Bay and F region ionospheric echo detection with the Rankin Inlet and Inuvik SuperDARN radars. Radio Sci 49:1194–1205. https://doi.org/10.1002/2014RS005579

Koustov AV, Fiori RAD, Aboolizadeh Z (2015) Long-term variations in the intensity of polar cap plasma flows inferred from SuperDARN. J Geophys Res Space Phys 120:9722–9737. https://doi.org/10.1002/2015JA021625

Koustov AV, Ponomarenko PV, Graf CJ, Gillies RG, Themens DR (2018) Optimal F region electron density for the PolarDARN radar echo detection near the Resolute Bay zenith. Radio Sci 53:1002–1013. https://doi.org/10.1029/2018RS006566

Lamarche LJ, Makarevich RA (2015) Solar control of F region radar backscatter: further insights from observations in the southern polar cap. J Geophys Res Space Phys 120:9875–9890. https://doi.org/10.1002/2015JA021663

MacDougall JW, Jayachandran PT, Plane JM (2000) Polar cap sporadic-E, Part 1, Observations. J Atmos Solar Terr Phys 62:1155–1167. https://doi.org/10.1016/S1364-6826(00)00093-6

Makarevich RA, Forsythe VV, Kellerman AC (2015) Electric field control of E region coherent echoes: evidence from radar observations at the South Pole. J Geophys Res Space Phys 120:2148–2165. https://doi.org/10.1002/2014JA020844

Milan SE, Yeoman TK, Lester M, Thomas EC, Jones TB (1997) Initial backscatter occurrence statistics for the CUTLASS HF radars. Ann Geophys 15:703–718. https://doi.org/10.1007/s00585-997-0703-0

Milan SE, Davies JA, Lester M (1999) Coherent HF radar backscatter characteristics associated with auroral forms identified by incoherent radar techniques: a comparison of CUTLASS and EISCAT observations. J Geophys Res Space Phys 104:22591–22604. https://doi.org/10.1029/1999JA900277

Nishitani N, Ruohoniemi JM, Lester M, Baker JBH, Koustov AV, Shepherd SG, Chisham G, Hori T, Thomas EG, Makarevich RA, Marchaudon A, Ponomarenko P, Wild J, Milan S, Bristow WA, Devlin J, Miller E, Greenwald RA, Ogawa T, Kikuchi T (2019) Review of the accomplishments of mid-latitude Super Dual Auroral Radar Network (SuperDARN) HF radars. Progr Earth Planet Sci 6:27. https://doi.org/10.1186/s40645-019-0270-5

Ponomarenko PV, Maurice J-P, Hussey GC, Koustov AV (2010) HF ground scatter from the polar cap: ionospheric propagation and ground surface effects. J Geophys Res Space Phys 115:A10310. https://doi.org/10.1029/2010JA015828

Ponomarenko PV, Koustov AV, St-Maurice J-P, Wiid J (2011) Monitoring the F-region peak electron density using HF backscatter interferometry. Geophys Res Lett 38:L21102. https://doi.org/10.1029/2011GL049675

Prikryl P, Jayachandran PT, Mushini SC, Pokhotelov D, MacDougall JW, Donovan E, Spanswick E, St-Maurice J-P (2010) GPS TEC, scintillation and cycle

slips observed at high latitudes during solar minimum. Ann Geophys 28:1307–1316. https://doi.org/10.5194/angeo-28-1307-2010
Ruohoniemi JM, Baker KB (1998) Large-scale imaging of high-latitude convection with Super Dual Auroral Radar Network HF radar observations. J Geophys Res 103:20797–20811. https://doi.org/10.1029/98JA01288
Ruohoniemi JM, Greenwald RA (1997) Rates of scattering occurrence in routine HF radar observations during solar cycle maximum. Radio Sci 32:1051–1070. https://doi.org/10.1029/97RS00116
Schlegel K (1996) Coherent backscatter from ionospheric E-region plasma irregularities. J Atmos Solar-Terr Phys 58:933–941. https://doi.org/10.1016/0021-9169(95)00124-7
Themens DR, Jayachandran PT, Galkin I, Hall C (2017) The Empirical Canadian High Arctic Ionospheric Model (E-CHAIM): NmF2 and hmF2. J Geophys Res Space Phys 122:9015–9031. https://doi.org/10.1002/2017JA024398
Tsunoda RT (1988) High latitude irregularities: a review and synthesis. Rev Geophys 26:719–760. https://doi.org/10.1029/RG026i004p00719
Uspensky MV, Koustov AV, Sofko GJ, Koehler JA, Villain J-P, Hanuise C, Ruohoniemi JM, Williams PJS (1994) Ionospheric refraction effects in slant range profiles of auroral HF coherent echoes. Radio Sci 29:503–517. https://doi.org/10.1029/93RS03256
Villain J-P, Greenwald RA, Vickrey JF (1984) HF ray tracing at high latitudes using measured meridional electron density distributions. Radio Sci 19:359–374. https://doi.org/10.1029/RS019i001p00359

Publisher's Note

Springer Nature remains neutral with regard to jurisdictional claims in published maps and institutional affiliations.

Submit your manuscript to a SpringerOpen journal and benefit from:

► Convenient online submission
► Rigorous peer review
► Open access: articles freely available online
► High visibility within the field
► Retaining the copyright to your article

Submit your next manuscript at ► springeropen.com